

IMMERSED-INTERFACE FINITE-ELEMENT METHODS FOR ELLIPTIC INTERFACE PROBLEMS WITH NONHOMOGENEOUS JUMP CONDITIONS*

YAN GONG[†], BO LI[‡], AND ZHILIN LI[§]

Abstract. In this work, a class of new finite-element methods, called *immersed-interface finite-element methods*, is developed to solve elliptic interface problems with nonhomogeneous jump conditions. Simple non-body-fitted meshes are used. A single function that satisfies the same nonhomogeneous jump conditions is constructed using a level-set representation of the interface. With such a function, the discontinuities across the interface in the solution and flux are removed, and an equivalent elliptic interface problem with homogeneous jump conditions is formulated. Special finite-element basis functions are constructed for nodal points near the interface to satisfy the homogeneous jump conditions. Error analysis and numerical tests are presented to demonstrate that such methods have an optimal convergence rate. These methods are designed as an efficient component of the finite-element level-set methodology for fast simulation of interface dynamics that does not require remeshing.

Key words. elliptic interface problems, nonhomogeneous jump conditions, immersed-interface finite-element method, level-set functions, error estimates

AMS subject classification. 65N30

DOI. 10.1137/060666482

1. Introduction. We consider numerical solution of the elliptic interface problem

$$(1.1) \quad -\nabla \cdot \beta^- \nabla u = f \quad \text{in } \Omega^-,$$

$$(1.2) \quad -\nabla \cdot \beta^+ \nabla u = f \quad \text{in } \Omega^+,$$

$$(1.3) \quad [u]_\Gamma = w,$$

$$(1.4) \quad \left[\beta \frac{\partial u}{\partial n} \right]_\Gamma = Q,$$

$$(1.5) \quad u = g \quad \text{on } \partial\Omega.$$

Here, $\Omega \subset \mathbb{R}^2$ is a bounded domain with its boundary $\partial\Omega$. Both Ω^- and Ω^+ are subdomains of Ω such that $\Omega^- \cap \Omega^+ = \emptyset$ and $\overline{\Omega^-} \cup \overline{\Omega^+} = \overline{\Omega}$, where an overline denotes the

*Received by the editors August 1, 2006; accepted for publication (in revised form) September 11, 2007; published electronically January 30, 2008.

<http://www.siam.org/journals/sinum/46-1/66648.html>

[†]Department of Mathematics, North Carolina State University, Raleigh, NC 27695-8205 (ygong@ncsu.edu).

[‡]Department of Mathematics, University of California, San Diego, 9500 Gilman Drive, Mail code: 0112, La Jolla, CA 92093-0112 (bli@math.ucsd.edu). This author's work was partially supported by the National Science Foundation through grant DMS-0451466 and the Department of Energy through grant DE-FG02-05ER25707.

[§]Center for Research in Scientific Computation and Department of Mathematics, North Carolina State University, Raleigh, NC 27695-8205 (zhilin@math.ncsu.edu). This author's work was partially supported by the National Science Foundation/National Institutes of Health through grant 0201094, ARO grant 49308-MA, AFSOR grant FA9550-06-1-024, National Science Foundation grant DMS-0412654, and the State Key Laboratory of Scientific and Engineering Computing of Chinese Academy of Sciences (summer, 2006).

closure; see Figure 1.1 for an illustration. For simplicity, we assume that $\overline{\Omega^-} \cap \partial\Omega = \emptyset$. We denote $\Gamma = \overline{\Omega^-} \cap \overline{\Omega^+}$ and call it the *interface* separating Ω^- and Ω^+ . We shall assume that Γ is sufficiently smooth. We also denote by n the unit vector normal to Γ pointing from Ω^- to Ω^+ , or the unit exterior normal to $\partial\Omega$, and by $\partial/\partial n$ or ∂_n the corresponding normal derivative.

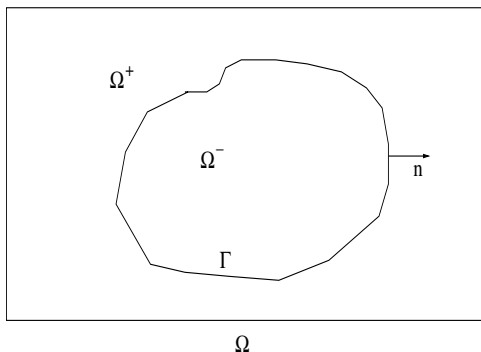


FIG. 1.1. The geometry of an elliptic interface problem.

All the functions $\beta, f : \Omega \rightarrow \mathbb{R}$, $w, Q : \Gamma \rightarrow \mathbb{R}$, and $g : \partial\Omega \rightarrow \mathbb{R}$ are given. As usual, for any function $\xi : \Omega \rightarrow \mathbb{R}$, we denote the restrictions of ξ on Ω^- and Ω^+ by

$$\xi^- = \xi|_{\Omega^-} \quad \text{and} \quad \xi^+ = \xi|_{\Omega^+},$$

respectively, and we denote by

$$[\xi]_{\Gamma}(x) = \lim_{y \rightarrow x, y \in \Omega^+} \xi^+(y) - \lim_{y \rightarrow x, y \in \Omega^-} \xi^-(y)$$

the jump of ξ across the interface Γ at $x \in \Gamma$, when the unique limiting values on Γ of ξ from both sides of Γ exist. We assume that β^- and β^+ are smooth and bounded on Ω^- and Ω^+ , respectively,

$$(1.6) \quad \beta(x) \geq \beta_0 \quad \forall x \in \Omega,$$

for some constant $\beta_0 > 0$, $f \in L^2(\Omega)$, all w, Q , and g are smooth and bounded.

Equations (1.3) and (1.4) are nonhomogeneous interface or jump conditions. Elliptic interface problems (1.1)–(1.5) with such jump conditions arise in many areas. For example, in a Burton–Cabrera–Frank-type model for epitaxial growth of thin films, the adatom (adsorbed atom) density that solves the diffusion equation on terraces, and the corresponding flux, can have jumps across interfaces that represent atomic steps [3, 5, 6]. Another example is that the reaction potential of electrostatics of a solvation energy satisfies a nonhomogeneous jump condition for the flux [13].

If the jump conditions are homogeneous, i.e., $w = 0$ and $Q = 0$ on Γ (cf. (1.3) and (1.4)), then the problem (1.1)–(1.5) is equivalent to that of finding $u \in H^1(\Omega)$ with $u = g$ on $\partial\Omega$ such that

$$\int_{\Omega} \beta \nabla u \cdot \nabla v \, dx = \int_{\Omega} f v \, dx \quad \forall v \in H_0^1(\Omega).$$

In general, we can extend the nonhomogeneous jump $w : \Gamma \rightarrow \mathbb{R}$ to a piecewise smooth function $\hat{w} : \Omega \rightarrow \mathbb{R}$ such that

$$[\hat{w}]_{\Gamma} = w \quad \text{and} \quad \hat{w} = g \quad \text{on} \quad \partial\Omega.$$

Then, the problem (1.1)–(1.5) is equivalent to the problem for $u = q + \hat{w}$ with $q \in H_0^1(\Omega)$ uniquely determined by

$$(1.7) \quad \int_{\Omega} \beta \nabla q \cdot \nabla v \, dx = \int_{\Omega} f v \, dx - \int_{\Gamma} Q v \, ds - \int_{\Omega} \beta \nabla \hat{w} \cdot \nabla v \, dx \quad \forall v \in H_0^1(\Omega).$$

In a standard body-fitted finite-element method for solving the problem in the weak formulation (1.7), the interface is covered by a low dimensional finite-element mesh, and the extension of $w : \Gamma \rightarrow \mathbb{R}$ to $\hat{w} : \Omega \rightarrow \mathbb{R}$ can be made by finite-element approximations.

In this work, we develop a class of finite-element methods based on non-body-fitted finite-element meshes to solve the elliptic interface problem (1.1)–(1.5). Such a method has the following distinguished features.

- (a) A fixed finite-element mesh that allows the interface to cut through edges of elements is used.
- (b) Both the jumps $w : \Gamma \rightarrow \mathbb{R}$ and $Q : \Gamma \rightarrow \mathbb{R}$ are extended locally by a single function using a level-set representation of the interface Γ . The extensions are necessary to transfer the original problem to a new one with homogeneous jump conditions so that the immersed finite-element methods developed in [18] can be applied. The new methods make it possible to maintain second order accuracy on the elements near the interface; see sections 2 and 5.
- (c) Special finite-element basis functions for nodal points near the interface are constructed to satisfy the homogeneous jump conditions; see section 4.
- (d) The resulting linear system of discretization is symmetric positive definite.
- (e) Optimal convergence rates, the same as those for a body-fitted finite-element method, are achieved; see section 3 for basic error estimates and section 6 for numerical results on such convergence properties.

Our methods incorporate the finite-element discretization into the framework of an immersed-interface method for interface problems, and we therefore call them *immersed-interface finite-element methods*. The basic idea of an immersed-interface method is to incorporate the jump conditions in constructing basis functions. In a finite-difference immersed-interface method, the jump conditions are enforced through finite-difference equations on grid points near the interface. In our immersed-interface finite-element methods, the jump conditions are enforced through the construction of special finite-element basis functions that satisfy the homogeneous interface conditions. Clearly, such basis functions depend on the interface location and the jump w . Some of the related work can be found in [7, 12].

The development of our methods is strongly motivated by the need for a fast and accurate solver of elliptic interface problems that is required in each time step in a long-time level-set simulation of interface dynamics without remeshing. Such simulation has been a powerful numerical approach in understanding material properties, biological processes, and many other important phenomena in science and engineering [20, 21, 22].

The finite-element spaces constructed in this paper are conforming ones that contain piecewise P_1 polynomials. The interpolation error is therefore of second order. If the solution to the elliptic interface problem is piecewise smooth, or, more precisely, $u^{\pm} \in C^2(\overline{\Omega^{\pm}})$, which is true for many applications, then the standard convergence results are true for our finite-element methods. This means that our finite-element solution is first order accurate in the H^1 norm and second order accurate in the L^2 norm. In this work, we construct only some two-dimensional linear and quadratic

triangular immersed-interface finite elements. However, our framework described here can be used for high order immersed-interface finite elements and for more general elliptic interface problems in two and three space dimensions.

We use the zero level set of a Lipschitz continuous function particularly, a good approximation of the signed distance function, to represent the interface Γ . For such a level-set function, the interface can cut the interface only once between two grid lines. The resolution of the interface Γ is determined by the level-set function. We note that there are plenty of discussions in the literature about how to construct the level-set function for an interface Γ ; see, e.g., [20, 22]. If the interface is complicated in reference to a mesh, then it may not be resolved well by the level-set function. Consequently, the finite-element solution obtained from our method may not resolve all the fine details of the solution. A finer mesh is then needed to resolve the geometry and the solution.

Our work combines the development of a new formulation of underlying problems, construction of new elements, basic error estimates, and numerical experiments. The analysis in our work focuses on two parts: one is the algorithm of removing source singularities, and the other is the interpolation error estimate for some of the immersed-interface finite-element approximations. We have not tried to deal in this paper with the analysis of other errors, such as those of the approximation of the interface Γ by Γ_h , numerical quadrature, round-off errors, etc.

In section 2, we present a new weak formulation of the elliptic interface problem (1.1)–(1.5) with a special treatment of nonhomogeneous jump conditions. In section 3, we describe the framework of our immersed-interface finite-element methods and provide basic error estimates. In section 4, we construct several linear or quadratic immersed-interface finite-element spaces and obtain their corresponding interpolation errors. In section 5, we give some details of implementation of our methods. In section 6, we present numerical results. Finally, in section 7, we draw conclusions.

2. Weak formulation. We first review the level-set representation of the interface Γ which is assumed to be smooth. Let $\varphi : \Omega \rightarrow \mathbb{R}$ be a continuous function that satisfies

$$(2.1) \quad \varphi(x) \begin{cases} < 0 & \text{if } x \in \Omega^-, \\ = 0 & \text{if } x \in \Gamma, \\ > 0 & \text{if } x \in \Omega^+. \end{cases}$$

We call such a function $\varphi : \Omega \rightarrow \mathbb{R}$ a *level-set function* that represents the interface Γ . For $\rho > 0$, we denote the ρ -neighborhood of Γ in Ω by

$$N(\Gamma, \rho) = \{x \in \Omega : \text{dist}(x, \Gamma) < \rho\},$$

where $\text{dist}(x, \Gamma)$ is the distance from x to Γ . We assume that there exists $\rho_0 > 0$ such that $N(\Gamma, \rho_0) \subset \Omega$, and

$$(2.2) \quad \varphi \text{ is smooth and } |\nabla\varphi| > 0 \text{ in } N(\Gamma, \rho_0).$$

We note that the unit normal n to Γ , pointing from Ω^- to Ω^+ , is given by

$$(2.3) \quad n = \frac{\nabla\varphi}{|\nabla\varphi|}.$$

The signed distance function

$$\varphi(x) = \begin{cases} -\operatorname{dist}(x, \Gamma) & \text{if } x \in \Omega^-, \\ 0 & \text{if } x \in \Gamma, \\ +\operatorname{dist}(x, \Gamma) & \text{if } x \in \Omega^+ \end{cases}$$

is a typical level-set function that satisfies our assumptions.

We now turn to the description of our treatment of nonhomogeneous jump conditions. We first need the following lemma.

LEMMA 2.1. *Let $\rho > 0$ be small enough. Then, for any $x \in N(\Gamma, \rho)$, there exists a unique $\hat{x} \in \Gamma$ such that*

$$(2.4) \quad |x - \hat{x}| = \operatorname{dist}(x, \Gamma).$$

Moreover,

$$(2.5) \quad \frac{x - \hat{x}}{|x - \hat{x}|} = \begin{cases} -n(\hat{x}) & \text{if } x \in \Omega^-, \\ +n(\hat{x}) & \text{if } x \in \Omega^+, \end{cases}$$

where $n(\hat{x})$ is the unit normal to Γ at \hat{x} , pointing from Ω^- to Ω^+ .

Proof. Without loss of generality, let us assume that, in a local Cartesian coordinate system, $x = (0, 0)$ is the origin, and the interface nearby is a graph of a smooth function $\eta = \eta(s)$ that is nonzero for any s in a certain range. The distance from the origin to any point $(s, \eta(s))$ on the interface is then given by $\sqrt{I(s)} < \rho$ with

$$I(s) = s^2 + [\eta(s)]^2.$$

Setting $I'(s) = 0$, we get $\eta'(s) = -s/\eta(s)$. This implies (2.5), since $(-1, \eta'(s))$ is parallel to the normal at $(s, \eta(s))$. Moreover,

$$I''(s) = 2 + 2[\eta'(s)]^2 + 2\eta(s)\eta''(s)$$

is positive, since $I(s)$, and hence $\eta(s)$, is small enough, whenever $\rho > 0$ is small enough. Thus, there exists a unique s that minimizes $I(s)$. This implies the existence and uniqueness of \hat{x} that satisfies (2.4). \square

In what follows, we fix $\rho_0 > 0$ as in (2.2). We let $\rho \in \mathbb{R}$ be given as in the above lemma and assume that $0 < \rho < \rho_0$. We define $w_\rho : \Omega \rightarrow \mathbb{R}$ and $Q_\rho : \Omega \rightarrow \mathbb{R}$ to be the extensions of $w : \Gamma \rightarrow \mathbb{R}$ and $Q : \Gamma \rightarrow \mathbb{R}$, respectively, that satisfy the following.

E1. Both w_ρ and Q_ρ are smooth on $\bar{\Omega}$.

E2. $w_\rho(x) = w(\hat{x})$ and $Q_\rho(x) = Q(\hat{x})$ for any $x \in N(\Gamma, \rho)$, where \hat{x} is defined as in Lemma 2.1.

E3. $w_\rho(x) = g(x)$ for any $x \in \partial\Omega$, and $Q_\rho(x) = 0$ for any $x \in \Omega \setminus N(\Gamma, \rho)$.

To see the existence of w_ρ , we first apply Lemma 2.1 to define a function, say, w_1 , by $w_1(x) = w(\hat{x})$ for any $x \in N(\Gamma, 2\rho)$ for $\rho > 0$ small enough, and $w_1 = 0$ elsewhere in Ω . Using the lifting operator [2, 11], there exists a smooth function, say, w_2 , on Ω such that the restriction of w_2 on $\partial\Omega$ is g . (The smoothness depends on that of $\partial\Omega$.) Now, assume that $N(\Gamma, 2\rho)$ and $A := N(\partial\Omega, \varepsilon) = \{x \in \Omega : \operatorname{dist}(x, \partial\Omega) < \varepsilon\}$ are disjoint for some small $\varepsilon > 0$. Then, by applying mollifiers to $w_1 + \chi_A w_2$, we obtain the desired w_ρ . The existence of Q_ρ is seen similarly.

We define $u_\rho : \Omega \rightarrow \mathbb{R}$ by

$$(2.6) \quad u_\rho(x) = \chi_{\Omega^+}(x) \left(w_\rho(x) + \frac{Q_\rho(x)}{\beta^+(x)} \frac{\varphi(x)}{|\nabla\varphi(x)|} \right) \quad \forall x \in \Omega,$$

where χ_{Ω^+} is the characteristic function of Ω^+ . Note by E3 that $Q_\rho = 0$ outside $N(\Gamma, \rho_0)$ in which φ may not be smooth. Thus, implicitly, the second term in u_ρ is defined to be 0 outside $N(\Gamma, \rho_0)$.

The following statement summarizes some useful properties of $u_\rho : \Omega \rightarrow \mathbb{R}$.

LEMMA 2.2. *Both u_ρ^- and u_ρ^+ are smooth on Ω^- and Ω^+ , respectively. Moreover, $u_\rho = g$ on $\partial\Omega$, and*

$$[u_\rho]_\Gamma = w, \quad \left[\beta \frac{\partial u_\rho}{\partial n} \right]_\Gamma = Q.$$

Proof. Since β^+ is smooth and bounded on Ω^+ , it follows from (1.6), E1, and (2.2) that u_ρ^+ is smooth on Ω^+ . Obviously, $u_\rho^- = 0$ is smooth on Ω^- . By E3, $u_\rho = g$ on $\partial\Omega$. By (2.1) and E2,

$$[u_\rho]_\Gamma = u_\rho^+ - u_\rho^- = w.$$

Now, fix $x \in \Gamma$. It follows from Lemma 2.1 and E2 that $\partial_n w_\rho = 0$. Moreover, $\varphi(x) = 0$ by (2.1). Therefore, for any $x \in \Gamma$, we obtain by E2, (2.6), (2.3), and the fact that $\varphi(x) = 0$ that

$$\begin{aligned} \left[\beta(x) \frac{\partial u_\rho(x)}{\partial n} \right]_\Gamma &= \beta^+(x) \frac{\partial u_\rho^+(x)}{\partial n} \\ &= \beta^+(x) \frac{\partial w_\rho(x)}{\partial n} + \beta^+(x) \frac{\partial}{\partial n} \left(\frac{Q_\rho(x)}{\beta^+(x) |\nabla\varphi(x)|} \right) \varphi(x) + \frac{Q_\rho(x)}{|\nabla\varphi(x)|} \frac{\partial \varphi(x)}{\partial n} \\ &= Q(x) \frac{n(x) \cdot \nabla\varphi(x)}{|\nabla\varphi(x)|} \\ &= Q(x). \end{aligned}$$

The proof is completed. \square

THEOREM 2.3. *There exists a unique $q \in H_0^1(\Omega)$ such that*

$$(2.7) \quad \int_\Omega \beta \nabla q \cdot \nabla v \, dx = \int_\Omega f v \, dx - \int_\Gamma Q v \, ds - \int_{\Omega^+} \beta^+ \nabla u_\rho \cdot \nabla v \, dx \quad \forall v \in H_0^1(\Omega).$$

This is equivalent to

$$(2.8) \quad \int_\Omega \beta \nabla q \cdot \nabla v \, dx = \int_\Omega f v \, dx + \int_{\Omega^+} (\nabla \cdot \beta^+ \nabla u_\rho) v \, dx \quad \forall v \in H_0^1(\Omega).$$

Moreover, $u = q + u_\rho$ solves the problem (1.1)–(1.5). In particular, $q \in H_0^1(\Omega)$ satisfies the homogeneous jump conditions

$$(2.9) \quad [q]_\Gamma = 0 \quad \text{and} \quad \left[\beta \frac{\partial q}{\partial n} \right]_\Gamma = 0.$$

Proof. Note that the line integral in (2.7) defines a continuous, linear functional on $H_0^1(\Omega)$. The existence and uniqueness of $q \in H_0^1(\Omega)$ satisfying (2.7) follow therefore

from the Lax–Milgram theorem. By integration by parts, (2.6), and Lemma 2.2, we imply that (2.7) and (2.8) are equivalent.

Choosing $v \in H_0^1(\Omega)$ with $\text{supp } v \subset \Omega^-$ and $\text{supp } v \subset \Omega^+$, respectively, applying the regularity theory of elliptic problems, we obtain from (2.7) that $u = q + u_\rho$ satisfies (1.1) and (1.2). The jump condition (1.3) follows from Lemma 2.2. Now, integrating by parts, we obtain by (1.1), (1.2), (2.6), and (2.7) that

$$\int_{\Gamma} \left(\left[\beta \frac{\partial u}{\partial n} \right]_{\Gamma} - Q \right) v \, ds = 0 \quad \forall v \in H_0^1(\Omega).$$

This leads to (1.4). Clearly, the function $u = q + u_\rho$ satisfies (1.5).

Finally, since $q = u - u_\rho$, we have

$$[q]_{\Gamma} = [u]_{\Gamma} - [u_\rho]_{\Gamma} = w - w = 0$$

from (1.3) and Lemma 2.2. We also have

$$\left[\beta \frac{\partial q}{\partial n} \right]_{\Gamma} = \left[\beta \frac{\partial u}{\partial n} \right]_{\Gamma} - \left[\beta \frac{\partial u_\rho}{\partial n} \right]_{\Gamma} = Q - Q = 0$$

from (1.4) and Lemma 2.2. \square

3. Immersed-interface finite-element approximations. In this section, we first state practically reasonable assumptions on how the interface can cut edges of elements in a finite-element mesh. We then define immersed-interface finite-element approximations of our underlying problem formulated in Theorem 2.3. Finally, we give rigorous error estimates for our method.

Let \mathcal{T}_h be a finite-element mesh with mesh size h that covers $\bar{\Omega}$. We assume that the elements in \mathcal{T}_h are all triangles. For simplicity, we shall assume that Ω is a convex polygonal domain and the mesh covers $\bar{\Omega}$ exactly. Standard finite-element techniques can be applied to treat a curved boundary without affecting our approximation properties. We remark that in practice the computational domain Ω can often be chosen as a rectangular domain with sides parallel to the coordinate axes; and the finite-element mesh can be uniform.

We call an element $T \in \mathcal{T}_h$ an *interface element* if $\Gamma \cap \text{int } T \neq \emptyset$. Note that an element is a noninterface element if one of its edges is part of the interface. We assume, for any interface element $T \in \mathcal{T}_h$, that the set $\Gamma \cap \partial T$ consists of exactly two points that are on different edges of T .

We define an immersed-interface finite-element space V_h with respect to the mesh \mathcal{T}_h to be a finitely dimensional subspace of $L^2(\Omega)$ that consists of all the linear combinations of the corresponding basis functions ϕ_1, \dots, ϕ_N for some integer $N \geq 1$:

$$(3.1) \quad V_h = \text{span} \{ \phi_1, \dots, \phi_N \}.$$

The basis functions are the usual finite-element basis functions on a noninterface element and are piecewise polynomials on each interface element that is determined by the element and the interface Γ . All the basis functions satisfy the homogeneous jump conditions for both the function and flux. Moreover, there exists an interpolation operator from some functional space to V_h that enjoys the usual approximation properties.

To be more precise, we define a *conforming immersed-interface finite-element space* V_h for the approximation of a second order elliptic interface problem to be a subspace of $H^1(\Omega)$ that satisfies the following properties.

- FE1. All the functions in V_h restricted onto the union of all noninterface elements form a usual finite-element space of piecewise polynomials of degree $\leq k$ for some integer $k \geq 1$, such as a P_k -type Lagrange finite-element space when \mathcal{T}_h is a triangular mesh, or a Q_k - or Q'_k -type Lagrange finite-element space when \mathcal{T}_h is a quadrilateral mesh [4, 8]. On each interface element $T \in \mathcal{T}_h$, all functions in V_h are piecewise polynomials. The support of each basis function is a union of a few elements.
- FE2. All the basis functions, and hence all the functions in V_h , satisfy the homogeneous jump conditions

$$(3.2) \quad [v_h]_{\Gamma_h} = 0 \quad \text{and} \quad \left[\beta(\hat{x}) \frac{\partial v_h}{\partial n} \right]_{\Gamma_h} = 0 \quad \forall v_h \in V_h,$$

where Γ_h denotes the union of line segments approximating the interface Γ , and the normal derivatives of $v_h \in V_h$ from each side of the interface are assumed to exist; \hat{x} is the orthogonal projection on the interface of the midpoint of Γ_h within the triangle.¹ Note that $[\beta(\hat{x}) \frac{\partial v_h}{\partial n}]_{\Gamma_h} = \beta^+(\hat{x}) \frac{\partial v_h^+}{\partial n} - \beta^-(\hat{x}) \frac{\partial v_h^-}{\partial n}$.

- FE3. There exists an interpolation operator $I_h : D(\Omega) \rightarrow V_h$ such that

$$(3.3) \quad \|I_h v - v\|_{H^1(\Omega)} \leq Ch^{\sigma(k)} \|v\|_{H^{k+1}(\Omega \setminus \Gamma)} \quad \forall v \in D(\Omega),$$

where $D(\Omega) \subset H^1(\Omega)$ is an infinite-dimensional space of functions that are smooth and bounded on both Ω^- and Ω^+ , respectively, \bar{k} is a constant such that $0 < \sigma(k) \leq k$, and $C > 0$ denotes a generic constant independent of h and v .

The homogeneous jump condition for $v_h \in V_h$ in (3.2) is a consequence of the fact that $V_h \subset H^1(\Omega)$. Often the interpolation error in FE3 can be the same as usual, i.e., $\bar{k} = k$. But, it can be slightly worse due to the approximation of Γ by Γ_h .

We can similarly define a *nonconforming immersed-interface finite-element* space $V_h \subset L^\infty(\Omega)$ with $V_h \not\subset H^1(\Omega)$. For a nonconforming immersed-interface finite-element space V_h that is used to solve our underlying problem with the boundary condition (1.5), we also need to assume that a discrete Poincaré inequality,

$$\|v_h\|_{L^2(\Omega)}^2 \leq C \sum_{T \in \mathcal{T}_h} \|\nabla v_h\|_{L^2(T \setminus \Gamma_h)}^2 \quad \forall v_h \in V_h,$$

is satisfied. Several examples of conforming and nonconforming, linear or quadratic, immersed-interface finite elements will be presented in the next section.

We consider now immersed-interface finite-element approximations of the solution $q \in H_0^1(\Omega)$ defined by (2.7). Let $u_\rho : \Omega \rightarrow \mathbb{R}$ be as given in (2.6) for some $\rho > 0$ small enough. Now let $V_h \subset H_0^1(\Omega)$ be a conforming immersed-interface finite-element space of piecewise polynomials of degree $\leq k$ as in FE1–FE3 that accounts for the boundary condition (1.5). To be precise, we assume in our analysis below that the domain of the interpolation operator I_h is

$$D(\Omega) = \left\{ v \in H_0^1(\Omega) : v^- \in H^{k+1}(\Omega^-) \cap C(\overline{\Omega^-}) \text{ and } v^+ \in H^{k+1}(\Omega^+) \cap C(\overline{\Omega^+}) \right\}.$$

¹Alternatively, we can approximate $\beta^\pm(\hat{x})$ using $\beta^\pm(\hat{X})$, where $\hat{X} \in \Gamma \cap \mathcal{T}_h$ is any point on the interface and in the triangle.

THEOREM 3.1. *There exists a unique $q_h \in V_h$ such that*

$$(3.4) \quad \int_{\Omega} \beta \nabla q_h \cdot \nabla v_h \, dx = \int_{\Omega} f v_h \, dx + \int_{\Omega^+} (\nabla \cdot \beta^+ \nabla u_{\rho}) v_h \, dx \quad \forall v \in V_h.$$

Moreover, if the solution $q \in H_0^1(\Omega)$ of (2.7) satisfies that $q^- \in H^{k+1}(\Omega^-) \cap C(\overline{\Omega^-})$ and $q^+ \in H^{k+1}(\Omega^+) \cap C(\overline{\Omega^+})$, then

$$(3.5) \quad \|q - q_h\|_{H^1(\Omega)} \leq Ch^{\sigma(k)} \|q\|_{H^{k+1}(\Omega \setminus \Gamma)},$$

$$(3.6) \quad \|q - q_h\|_{L^2(\Omega)} \leq Ch^{\sigma(k)+\sigma(1)} \|q\|_{H^{k+1}(\Omega \setminus \Gamma)},$$

where $\sigma(k)$ is defined in FE3 and $C > 0$ is a constant independent of h and q .

Proof. Since $V_h \subset H_0^1(\Omega)$, the existence and uniqueness of $q_h \in V_h$ satisfying (3.4) follow from the Lax–Milgram theorem. Moreover, by (2.8), which is equivalent to (2.7) by Theorem 2.3, and (3.4), we obtain

$$(3.7) \quad \int_{\Omega} \beta \nabla (q - q_h) \cdot \nabla v_h \, dx = 0 \quad \forall v_h \in V_h.$$

The error estimate (3.5) can be obtained by a standard argument using a Poincaré inequality, the ellipticity indicated by (1.6), the error equation (3.7), and the interpolation error estimate (3.3); see [4, 8].

To obtain the L^2 error estimate (3.6), we use the standard dual argument (cf., e.g., [4, 8]) with slight modification taking care of the lack of global regularity of a solution. Let $r \in H_0^1(\Omega)$ be the unique function satisfying

$$(3.8) \quad \int_{\Omega} \beta \nabla r \cdot \nabla v \, dx = \int_{\Omega} (q - q_h) v \, dx \quad \forall v \in H_0^1(\Omega).$$

Since β^- and β^+ are smooth and bounded in Ω^- and Ω^+ , respectively, we see that $r^- \in H^2(\Omega)$ and $r^+ \in H^2(\Omega)$. Moreover, it follows from (3.8) that $[\beta \partial_n r]_{\Gamma} = 0$. Therefore, we have (cf. Theorem 2.1 in [7]) that

$$(3.9) \quad \|r^{\pm}\|_{H^2(\Omega^{\pm})} \leq C \|q - q_h\|_{L^2(\Omega)}.$$

Setting $v = q - q_h \in H_0^1(\Omega)$ in (3.8), we have by (3.8), (3.7) with $v_n = I_h r$, the Cauchy–Schwarz inequality, (3.3) with $k = 1$, (3.5), and (3.9) that

$$\begin{aligned} \|q - q_h\|_{L^2(\Omega)}^2 &= \int_{\Omega} \beta \nabla r \cdot \nabla (q - q_h) \, dx \\ &= \int_{\Omega} \beta \nabla (r - I_h r) \cdot \nabla (q - q_h) \, dx \\ &\leq C \|r - I_h r\|_{H^1(\Omega)} \|q - q_h\|_{H^1(\Omega)} \\ &\leq Ch^{\sigma(k)+\sigma(1)} \|r\|_{H^2(\Omega \setminus \Gamma)} \|q\|_{H^{k+1}(\Omega \setminus \Gamma)} \\ &\leq Ch^{\sigma(k)+\sigma(1)} \|q\|_{H^{k+1}(\Omega \setminus \Gamma)} \|q - q_h\|_{L^2(\Omega)}, \end{aligned}$$

leading to (3.6). \square

We remark that the removal of both jumps w and Q using a single function leads to finite-element equation (3.4) which does not involve line integrals as in (2.7). This much simplifies numerical implementation.

4. Construction of basis functions. We now describe how to construct some new classes of triangular immersed-interface finite-element basis functions that satisfy the homogeneous jump conditions.

Let z_1, \dots, z_N be all the vertices of triangular elements in the mesh \mathcal{T}_h . We define our linear or quadratic linear immersed-interface finite-element basis functions ϕ_i associated with z_i ($i = 1, \dots, N$) to be functions on Ω that satisfy the following properties.

- B1. Each ϕ_i ($1 \leq i \leq N$) is linear on a noninterface element and is piecewise linear or quadratic on an interface element.
- B2. $\phi_i(z_j) = \delta_{ij}$ for $i, j = 1, \dots, N$, where $\delta_{ij} = 1$ if $i = j$ and 0 if $i \neq j$.
- B3. All ϕ_i ($1 \leq i \leq N$) satisfy the approximate homogeneous jump conditions

$$[\phi_i]_{\Gamma_h} = 0, \quad \left[\beta(\hat{x}) \frac{\partial \phi_i}{\partial n} \right]_{\Gamma_h} = 0.$$

The corresponding finite-element space V_h is given by (3.1).

We call a vertex an *irregular vertex* or *irregular node* if it is a vertex of an interface element and a *regular vertex* or *regular node* otherwise. For a regular node z_i , we define ϕ_i to be the usual conforming linear finite-element basis function associated with z_i , i.e., $\phi_i \in C(\bar{\Omega}) \cap H_0^1(\Omega)$, ϕ_i is a linear polynomial on each element $T \in \mathcal{T}_h$, and $\phi_i(z_j) = \delta_{ij}$ for $j = 1, \dots, N$.

For an irregular node z_i , we construct the corresponding basis function by modifying the usual linear finite-element basis function to satisfy the properties B1–B3. We need only to construct a local basis (or shape) function on an interface element for an irregular node.

4.1. A nonconforming linear element. This nonconforming immersed-interface finite element was first constructed in [18]; see also [12]. We briefly review it, since it will be used to construct our new linear and quadratic elements.

Fix an interface element $T \in \mathcal{T}_h$; cf. Figure 4.1. As in the common practice, we approximate the interface in T , $\Gamma \cap T$, by a line segment connecting the intersections of the interface and the edges of the triangle T . This line segment is \overline{DE} in Figure 4.1. The line segment divides T into two parts T^+ and T^- , one triangular and the other quadrilateral. Note that there is a small region T_r in T ,

$$T_r = T - \Omega^+ \cap T^+ - \Omega^- \cap T^-,$$

whose area is of order $O(h^3)$.

We now consider the element T in Figure 4.1 as a reference interface element T and define local basis functions for each vertex of T . The local basis function for a general interface element in the mesh \mathcal{T}_h can be defined through the usual affine transformation. We denote

$$T = \{(x_1, x_2) : 0 \leq x_1 \leq h, \quad 0 \leq x_2 \leq hx_1 + x_2 \leq h\}$$

and assume that the coordinates at A, B, C, D , and E are

$$(0, h), \quad (0, 0), \quad (h, 0), \quad (0, y_1), \quad (h - y_2, y_2),$$

respectively; cf. Figure 4.1.

Each of the three local basis functions corresponding to the nodes A, B , or C takes value 1 at one node and 0 at the other two. Once the values at nodes A, B , and

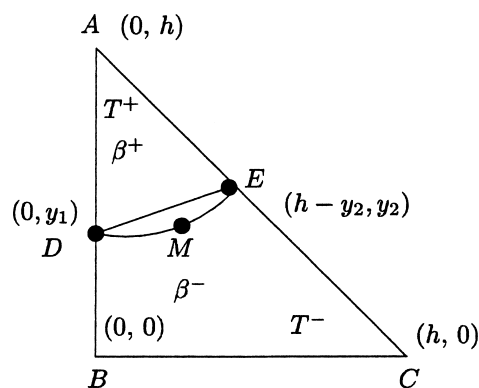


FIG. 4.1. A typical interface element $T = \triangle ABC$. The arc DME is the part of the interface Γ in T . It is approximated by the line segment \overline{DE} . $T^+ = \triangle ADE$, $T^- = T - T^+$, and T_r is the region enclosed by the \overline{DE} and the arc DME .

C are specified, a local nonconforming finite-element basis function ϕ for this interface triangle is determined by

$$(4.1) \quad \phi(x) = \begin{cases} \phi^+(x) = a_0 + a_1x_1 + a_2(x_2 - h) & \text{if } x = (x_1, x_2) \in T^+, \\ \phi^-(x) = b_0 + b_1x_1 + b_2x_2 & \text{if } x = (x_1, x_2) \in T^-. \end{cases}$$

The coefficients a_i and b_i ($i = 0, 1, 2$) are determined by the conditions (cf. [18])

$$(4.2) \quad \phi^+(D) = \phi^-(D), \quad \phi^+(E) = \phi^-(E), \quad \beta^+ \frac{\partial \phi^+}{\partial n} = \beta^- \frac{\partial \phi^-}{\partial n},$$

where n is the unit normal direction of the line segment \overline{DE} . It is shown in [18] that this function ϕ is uniquely determined. Note that basis functions defined in this way can be discontinuous across edges of interface elements. So, this defines a nonconforming finite element.

4.2. A conforming linear element. This conforming element was proposed in [18]. Both error estimates and numerical experiments in [18] show that the corresponding interpolation errors that can depend on an angle condition are of second order, which is optimal [18].

Let $T = \triangle ABC$ be an interface element; cf. Figure 4.2. As before, we assume that the interface meets edges of this element at D and E . To construct a local basis function that is globally continuous, we extend the previously defined basis function at the same node (vertex) to one more triangle along the interface (cf. Figure 4.2 (b)). We require that the local basis functions in two adjacent interface elements, such as $\triangle ABC$ and $\triangle AFB$, take the same value at the interface point on their common edge, such as the point D . This will achieve the global continuity of a basis function associated with an irregular node.

We construct a local basis function ϕ by assigning its values at the vertices A , B , C , F , and I , respectively. This construction consists of the following five steps.

- P1. Use the values at the nodes A , B , C , F , and I to construct the three nonconforming finite-element basis functions defined as in subsection 4.1 on the elements $\triangle ABC$, $\triangle AFB$, and $\triangle ACI$, respectively.

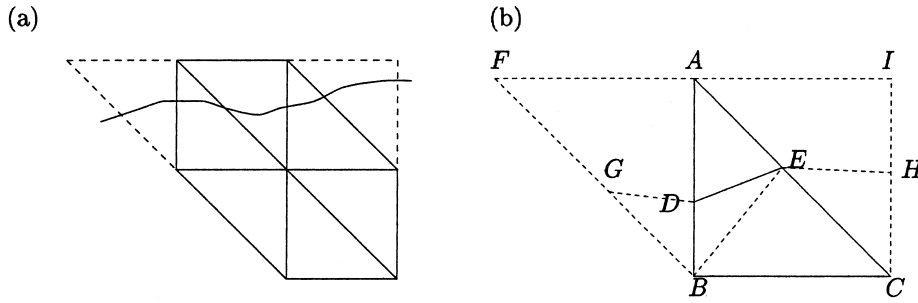


FIG. 4.2. (a) The support of a local basis function. (b) A diagram for the construction of a local basis function on $\triangle ABC$.

- P2. Set the value at D as the average of the values at D of the nonconforming piecewise linear basis functions defined on $\triangle ABC$ and $\triangle AFB$ constructed in P1.
- P3. Similarly, set the value at E as the average of values at E of the nonconforming piecewise linear basis functions defined on the elements $\triangle ABC$ and $\triangle ACI$ constructed in P1.
- P4. Partition the element $\triangle ABC$ into three subtriangles by an auxiliary line, say, line segment \overline{BE} , or \overline{DC} . We choose the auxiliary line in such a way that at least one of angles (or complimentary angles if the angle is more than $\pi/4$) is bigger than or equal to $\pi/2$.
- P5. Define the basis function to be the piecewise linear function in the three subtriangles determined by the values at the points A, B, C, D , and E .

For this type of conforming finite-element space and homogeneous jump conditions, i.e., $w = 0$ and $Q = 0$, we have the following error estimates of the interpolation function:

$$(4.3) \quad \|I_h u - u\|_\infty \leq Ch^2 \|D^2 u\|_{\infty, \Omega \setminus (\cup T_r)},$$

$$(4.4) \quad \|I_h u - u\|_{H^1(\Omega)} \leq Ch \|D^2 u\|_{\infty, \Omega \setminus (\cup T_r)},$$

assuming that $\beta(x)$ is a piecewise constant and the solution is piecewise smooth in Ω^- and Ω^+ , where $C > 0$ is a generic constant independent of h and $\cup T_r$ is the region of mismatched regions between Γ and Γ_h ; see [18] for the proof.

4.3. A conforming quadratic element. We now construct a conforming quadratic element. As before, the basis functions associated with regular nodes are the standard conforming linear finite-element basis functions. But, the basis functions associated with irregular nodes are piecewise quadratic. All the basis functions are globally continuous. The idea is to average the tangential derivatives in the construction in subsection 4.2. Referring the reader to Figure 4.2, we describe this procedure as follows.

- P1. Use the values at the nodes A, B, C, F , and I to construct the three nonconforming linear finite-element basis functions defined in subsection 4.1 on the elements $\triangle ABC$, $\triangle AFB$, and $\triangle ACI$, respectively.
- P2. Set the value at D as the average of the values at D of the nonconforming linear finite-element basis functions defined $\triangle ABC$ and $\triangle AFB$ constructed in P1. Assign the tangential derivative at D along AD to be the average of the values of the tangential derivatives (along AD) of the nonconforming

linear finite-element basis functions on ΔABC and ΔAFB constructed in P1. Similarly, assign the tangential derivative at D along DB as the average of the values of the tangential derivatives (along DB) of the nonconforming finite-element basis functions on ΔABC and ΔAFB constructed in P1.

- P3. Repeat to set the value at E as the average of values at E of the nonconforming linear finite-element basis functions defined on the elements ΔABC and ΔACI in P1. Also assign the tangential derivatives along AE and EC as the average of those from the nonconforming finite-element basis functions along the same edge.
- P4. Partition the element ΔABC into three subtriangles by an auxiliary line. We choose the auxiliary line in such a way that at least one of the angles (or complimentary angles if the angle is bigger than $\pi/4$) is bigger than or equal to $\pi/2$. In Figure 4.2, for example, the angles are $\angle EDB$, $\angle DEB$, and $\angle EBD$, where the complimentary angle of $\angle EDB$ is bigger than $\pi/4$.
- P5. Assign the tangential derivatives along DE and BE exactly the same (no average) as those from the nonconforming finite-element basis functions.
- P6. Set the values of the tangential derivatives along BE and BC exactly the same as those from the nonconforming finite-element basis function on ΔABC .
- P7. Define the basis function ψ_i to be the piecewise quadratic function in the three subtriangles determined by the values at the points A , B , C , D , and E , respectively, and the tangential derivatives from each side of the triangles; see Figure 4.3 for an illustration.

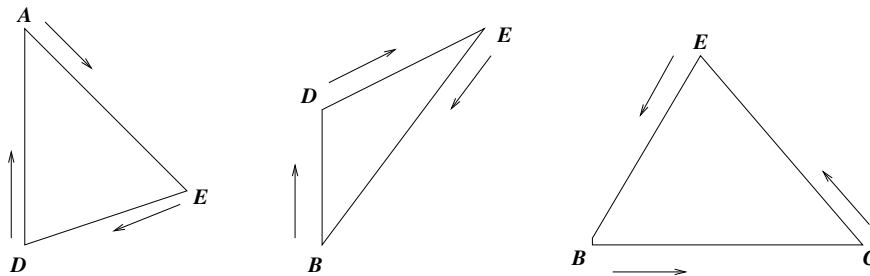


FIG. 4.3. Three triangles on which piecewise continuous quadratic functions can be determined. The symbol “ \longrightarrow ” indicates a tangential derivative.

We now give an error estimate for the interpolation error of this element for a given piecewise smooth function v . We first show that a quadratic function on a triangle is uniquely determined by its values at the three vertices and its tangential derivatives along the three sides at some particular points.

LEMMA 4.1. *Referring to the geometry in Figure 4.4, there is a unique quadratic polynomial*

$$(4.5) \quad I_h v(x, y) = v_A + a_{10}x + a_{01}y + a_{20}x^2 + a_{11}xy + a_{02}y^2$$

that interpolates the values of v_A , v_D , and v_E , and three tangential derivatives v'_{AE} , v'_{AD} , and v'_{ED} defined at the three vertices A , E , and D , respectively.

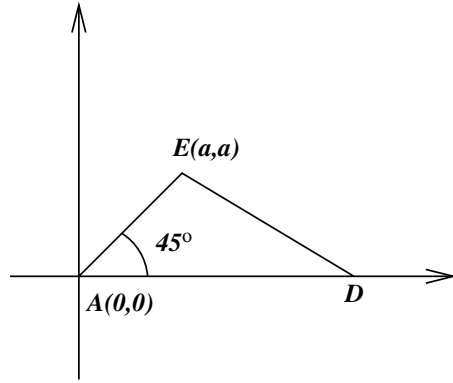


FIG. 4.4. An illustration of determining the quadratic interpolation function.

Proof. Using the undetermined coefficient method, we find the unique expression of the coefficients²

$$\begin{aligned}
 a_{10} &= \frac{\tilde{h}v'_{AD} + 2v_D - 2v_A}{\tilde{h}}, \\
 a_{01} &= -\frac{\tilde{h}v'_{AD} - \sqrt{2}v'_{AE}\tilde{h} + 2v_D - 2v_A}{\tilde{h}}, \\
 a_{20} &= -\frac{\tilde{h}v'_{AD} + v_D - v_A}{\tilde{h}^2}, \\
 a_{11} &= -\frac{-2\tilde{h}\alpha v'_{AD} - 2\alpha v_D + 2\alpha v_A + \tilde{h}^2 v'_{AD} + 2\tilde{h}v_D}{\tilde{h}^2\alpha} \\
 &\quad - \frac{\sqrt{\tilde{h}^2 - 2\tilde{h}\alpha + 2\alpha^2}v'_{ED}\tilde{h} + \tilde{h}\alpha\sqrt{2}v'_{AE} - 2\tilde{h}v_E}{\tilde{h}^2\alpha}, \\
 a_{02} &= \frac{\tilde{h}^2 v'_{AD}\alpha + 2\tilde{h}\alpha v_D - \tilde{h}^2\alpha\sqrt{2}v'_{AE} - \tilde{h}v'_{AD}\alpha^2 - \alpha^2 v_D + \alpha^2 v_A}{\tilde{h}^2\alpha^2} \\
 &\quad + \frac{v_E\tilde{h}^2 - v_A\tilde{h}^2 + \sqrt{\tilde{h}^2 - 2\tilde{h}\alpha + 2\alpha^2}v'_{ED}\tilde{h}\alpha + \tilde{h}\alpha^2\sqrt{2}v'_{AE} - 2v_E\tilde{h}\alpha}{\tilde{h}^2\alpha^2},
 \end{aligned}$$

where \tilde{h} is the distance from A to D , and the coordinates at E are (α, α) . \square

There are two steps in obtaining the interpolation error. First, the values of the quadratic function according to our algorithm at vertices either are directly copied from the conforming linear basis function (at the vertices of the right triangles) or are the average of values of the conforming linear basis function from the two adjacent triangles. Therefore, those values are $O(h^2)$ perturbations to v from the reference [18]. Similarly, the values of the tangential derivatives are $O(h)$ perturbations to that of v . Second, from the above reasoning, we can conclude that the values at the mid-points of each side of the triangle are $O(h^2)$ perturbations to v . Since the quadratic function can also be uniquely determined from its values at vertices and the three midpoints

²We use Maple to get the coefficients.

and it is insensitive to perturbations of those values (see [14]), we conclude that the interpolation function is an $O(h^2)$ perturbation to $v(x)$ in the entire triangle.

The second part of the argument is a direct consequence of the interpolation error estimate for the standard conforming P_2 finite element. The first part of the argument is a consequence of the following result.

LEMMA 4.2. *Let $a, b \in \mathbb{R}$ with $h := b - a > 0$. Let $v \in C^1[a, b]$. Then, there exists a unique quadratic polynomial p such that $p(a) = v(a)$, $p(b) = v(b)$, and $p'(a) = v'(a)$. Moreover, if v is smooth, then*

$$\begin{aligned}\|v - p\|_{L^\infty(a, b)} &\leq Ch^3, \\ \|v' - p'\|_{L^\infty(a, b)} &\leq Ch^2,\end{aligned}$$

where $C > 0$ is a constant independent of h .

Proof. Note that any quadratic polynomial q can be written as

$$q(x) = q(a) + q'(a)(x - a) + \frac{q(b) - q(a) - q'(a)(b - a)}{(b - a)^2} (x - a)^2.$$

Therefore, the unique quadratic polynomial that interpolates $v(a)$, $v(b)$, and $v'(a)$ is given by

$$p(x) = v(a) + v'(a)(x - a) + \frac{v(b) - v(a) - v'(a)(b - a)}{(b - a)^2} (x - a)^2.$$

Now an application of the Bramble–Hilbert lemma [8] concludes the proof. \square

The lemma is still true if we replace $p'(a)$ by $p'(b)$.

By the lemma, we see that if $p(a) = v(a) + O(h^2)$, $p(b) = v(b) + O(h^2)$, and $p'(a) = v'(a) + O(h)$, then $|v(x) - p(x)| = O(h^2)$ and $|v'(x) - p'(x)| = O(h)$ in the entire interval $[a, b]$ including the midpoint.

With the same local angle constraint given in [18] (e.g., at least one angle or complementary angle is larger than or equal to $\pi/4$), we have the following error estimates for the interpolation.

PROPOSITION 4.3. *Assume that $w = Q = 0$, $\beta(x)$ is a piecewise constant, and the solution u is piecewise C^2 , i.e., $u^\pm \in C(\bar{\Omega}^\pm)$. Then the following error estimates hold:*

$$(4.6) \quad \|I_h u - u\|_\infty \leq Ch^2 \|D^2 u\|_{\infty, \Omega \setminus \Sigma T_r},$$

$$(4.7) \quad \|I_h u - u\|_{H^1(\Omega)} \leq Ch \|D^2 u\|_{\infty, \Omega \setminus \Sigma T_r}.$$

For the conforming linear finite-element space, the proof is given in [18]. So we just need to discuss the conforming quadratic finite-element space. The proof of the first inequality is straightforward, as has been discussed above. The proof of the second inequality is quite technical and tedious with different geometric configurations. This proof, though, is quite similar to that for the nonconforming immersed finite-element method (cf. [18]); we give only a sketch here. Taking the geometry in Figure 4.4 as an example, we have analytic expression of the interpolation function given in Lemma 4.1 in terms of its values and the tangential derivatives (averaging those of the nonconforming interpolation function). From the analytic expression of the

interpolation, it is easy to get $\|\nabla I_h u - \nabla I_h \tilde{u}\|_\infty \leq Ch$, where $I_h \tilde{u}$ is any quadratic function when we perturb v_A, v_D , and v_E by $O(h^2)$, and v'_{AD}, v'_{AE} , and v'_{ED} by $O(h)$.

Our numerical tests reported in section 6 confirm such an estimate for the interpolation error. Note that, while the error bounds for the linear and quadratic basis functions are the same, numerical examples of our test problems show that the quadratic one behaves better numerically. Since the quadratic basis function is a conforming one, we can conclude that the finite-element solution is first order in the H^1 norm from the standard finite element theory.

Remark 1. Consider a uniform triangular mesh. For both conforming linear and conforming quadratic elements, the basis function ϕ_i associated with the i th node is nonzero only on the six surrounding triangular elements if the interface does not cut through any of these triangles. Otherwise, the support of a basis function includes two more triangular elements along the direction of the interface if the interface cuts through any of the surrounding triangle. A corresponding finite-difference scheme, however, generally has a nonstandard nine-point stencil.

Remark 2. If the coefficient β is continuous across the interface, i.e., $[\beta]_\Gamma = 0$, then both the linear and quadratic basis functions become the standard linear basis functions.

5. Implementation. In this section, we give details about the numerical extension of the jumps w and Q , the assembly of the stiffness matrix and load vector, and the evaluation of certain integrals on part of an interface element.

5.1. Numerical extension of the jumps w and Q . We use a Gaussian quadrature to compute the stiffness matrix and the load vector in each triangle $\triangle ADE, \triangle DEB$, and $\triangle BEC$ in Figure 4.2. Let x be such a Gaussian point which is close to the interface. We need to extend the jumps w and Q to this Gaussian point by the definition of w_ρ and Q_ρ given in E2 and E3 in section 2. This is done in two steps. The first step is to find an approximation of the orthogonal projection \hat{x} of x on the interface Γ ; see Lemma 2.1. The second step is to define the extensions of w and Q at x as $w(\hat{x})$ and $Q(\hat{x})$, respectively.

The orthogonal projection can be approximated by

$$\hat{x} = x + \alpha p,$$

where

$$p = \begin{bmatrix} \varphi_x(x) \\ \varphi_y(x) \end{bmatrix}.$$

Here, a subscript denotes a partial derivative. The scalar α is determined from the following quadratic equation:

$$\varphi(x) + (\nabla\varphi(x) \cdot p) \alpha + \frac{1}{2} (p^T \text{He}(\varphi(x)) p) \alpha^2 = 0,$$

where

$$p^T \text{He}(\varphi) p = \varphi_x^2 \varphi_{xx} + 2 \varphi_x \varphi_y \varphi_{xy} + \varphi_y^2 \varphi_{yy}.$$

The sign of α is chosen to be opposite that of $\varphi(x)$. If the underlying mesh is uniform, formulated from a Cartesian grid, then, the partial derivatives $\nabla\varphi(x)$ and the Hessian

matrix $\text{He}(\varphi)$ can be computed at x using the standard centered five-point finite-difference formula. Using the method above, the computed projections have third order accuracy.

Note that in our implementation, we use the orthogonal projections $\hat{x} \in \Gamma$. It is also possible to use the orthogonal projections $\hat{x} \in \Gamma_h$. The difference in the finite-element solution using the two different implementations is small since the area of the mismatched region $\sum T_r$ is small. If the level set function is the signed distance function, or a good approximation of the signed distance function, then the error in approximating \hat{x} would be $O(h^3)$; see [19]. We also refer the reader to [9, 10] for some of the recent discussions on computing orthogonal projections.

Note that when one uses a finite number of piecewise linear basis functions $\phi'_h s \in V_h$ to seek the finite-element solution, we have introduced an error in substituting $V = H^1(\Omega)$ by V_h which is often $O(h^2)$. Other approximating errors, such as numerical integration, approximating orthogonal projections, have little effect on the finite-element solutions as long as they are higher order terms of h^3 .

In practice, we need only to extend both jumps w and Q to $N(\Gamma, 2h)$, the $2h$ neighborhood of the interface Γ . This is described in (5.4), where the last two terms are identical but differ by a sign for noninterface triangles.

5.2. Assembly of stiffness matrix and load vector. On noninterface elements where the interface does not cut through, we can use the standard way in computing the contribution to the stiffness matrix and the load vector. On interface elements where the interface cuts through, we need to modify the load vector (the right-hand side); but the computation for the stiffness matrix remains the same as in the case of homogeneous jump conditions.

To fix this idea, let us focus on the quadratic conforming element (cf. subsection 4.3). We rewrite the finite-element equation (3.4) in terms of $u_h = q_h + u_\rho$:

$$(5.1) \quad \int_{\Omega} \beta \nabla u_h \cdot \nabla v_h \, dx = \int_{\Omega} f v_h \, dx + \int_{\Omega} \beta \nabla u_\rho \cdot \nabla v_h \, dx + \int_{\Omega} H(\varphi) \nabla \cdot (\beta \nabla \tilde{u}_\rho) v_h \, dx \quad \forall v_h \in V_h,$$

where H is the Heaviside function and \tilde{u}_ρ is given by

$$(5.2) \quad \tilde{u}_\rho(x) = w_\rho(x) + \frac{Q_\rho(x)}{\beta^+(x)} \frac{\varphi(x)}{|\nabla \varphi(x)|}, \quad x \in \Omega.$$

Note that \tilde{u}_ρ is smooth in a neighborhood of Γ and that $u_\rho = \chi_{\Omega^+} \tilde{u}_\rho$ and its corresponding flux have nonhomogeneous jumps across the interface.

Let $\{\phi_j(x)\}$ be the basis functions of the modified conforming finite-element space. Then, we define

$$(5.3) \quad u_h(x) = \begin{cases} \sum_j \alpha_j \phi_j(x) & \text{if } x \text{ belongs to a noninterface triangle,} \\ \sum_j \alpha_j \phi_j(x) + \sum_j u_\rho(x_j) \phi_j(x) & \text{otherwise,} \end{cases}$$

where $\phi_j(x)$ is the j th basis function centered at x_j . The left-hand side is exactly the same as in the case of the homogeneous jump condition. The entries of the stiffness matrix are

$$a_{ij} = \int_{\Omega} \beta \nabla \phi_i \cdot \nabla \phi_j \, dx.$$

Only the right-hand side of the system of equation needs to be modified for certain triangles near the interface.

At a noninterface triangle that is entirely in Ω^- , the last two terms of integration over the triangle are zero, since $H(\varphi(x)) = 0$ and $u_\rho = 0$. The situation is a little more complicated for triangles in Ω^+ . If all the nonzero basis functions over a triangle in Ω^+ have no support from interface triangles, then the last two terms in (5.1) are canceled out. To see this, let T_k be such a triangle, and let ϕ_l be such a basis function with Ω_l being its support. We have

$$\begin{aligned} & \int_{\Omega_l} \beta \nabla u_\rho \cdot \nabla \phi_l \, dx + \int_{\Omega_l} H(\varphi) \nabla \cdot (\beta \nabla \tilde{u}_\rho) \phi_l \, dx \\ &= \int_{\Omega_l} \beta \nabla u_\rho \cdot \nabla \phi_l \, dx + \int_{\Omega_l} \nabla \cdot (\beta \nabla \tilde{u}_\rho) \phi_l \, dx \\ &= \int_{\Omega_l} \beta \nabla u_\rho \cdot \nabla \phi_l \, dx + \int_{\partial \Omega_l} \frac{\partial \tilde{u}_\rho}{\partial n} \phi_l \, ds - \int_{\Omega_l} \beta \nabla \tilde{u}_\rho \cdot \nabla \phi_l \, dx = 0, \end{aligned}$$

since $\tilde{u}_\rho = u_\rho$ and $\phi_l = 0$ along $\partial \Omega_l$. In other words, the total contribution of the line integral along the boundary of each triangle summed up to be zero. The right-hand side of the load vector can be summarized as

$$(5.4) \quad F_i = \begin{cases} \int_{\Omega_i} f \phi_i \, dx & \text{if } \Omega^s(\phi_i) \cap \Gamma = \emptyset, \\ \int_{\Omega_i} f \phi_i \, dx + \int_{\Omega^s} H(\varphi) \nabla \cdot (\beta \nabla \tilde{u}_\rho) \phi_i \, dx \\ \quad + \sum_j u_\rho(x_j) \int_{\Omega_i} \beta \nabla \phi_i \cdot \nabla \phi_j \, dx & \text{otherwise,} \end{cases}$$

where $\Omega^s(\phi_i)$ is the support of ϕ_i .

5.3. Evaluation of $\int_{\Omega^s} H(\varphi) \nabla \cdot (\beta \nabla \tilde{u}_\rho) \phi_i \, dx$. Take Figure 4.1 as an example. There are two ways to evaluate the integral. One way is to use

$$(5.5) \quad \int_{T_j} H(\varphi) \nabla \cdot (\beta \nabla \tilde{u}_\rho) \phi_i \, dx = \int_{\partial \triangle ADE} \beta \frac{\partial \tilde{u}_\rho}{\partial n} \phi \, ds - \int_{\triangle ADE} \nabla \tilde{u}_\rho \cdot \nabla \phi \, dx.$$

The line integral is evaluated using a Gaussian quadrature formula or some other numerical quadrature.

The second approach is to evaluate the double integral directly over the triangle using a quadrature formula, say, the four-point formula [14]. The coefficient β is approximated by a constant in the triangle. In order to evaluate the values of the integrand at a given point x , we first find a square $[x_i, x_{i+1}] \times [y_j, y_{j+1}]$ that contains the point x . The Laplacian at the vertices $(x_{i\pm 1}, y_{j\pm 1})$ is computed using the standard three-point central finite difference formula. Finally, the Laplacian at the point x is interpolated using the bilinear interpolation; see [17].

6. Numerical results. We report two examples of numerical calculations using our conforming quadratic immersed-interface finite-element method. In each of the calculations, we used ITPACK [23] to solve the resulting linear system of equations.

Example 1. Homogeneous jump conditions. This example is from [18]. We consider the problem (1.1)–(1.5) with $\Omega = (-1, 1) \times (-1, 1)$, Γ being the circle centered at point $(0, 0)$ with radius $R = 0.5$, $\beta^- = 1$, and $\beta^+ = 100$. The source term $f(x, y)$ and the Dirichlet boundary data $u_0(x, y)$ are calculated from the exact solution $u(x, y)$:

$$u(x, y) = \begin{cases} \frac{r^3}{\beta^-} & \text{if } r \leq R, \\ \frac{r^3}{\beta^+} + \left(\frac{1}{\beta^-} - \frac{1}{\beta^+}\right) R^3 & \text{otherwise,} \end{cases}$$

where $r = \sqrt{x^2 + y^2}$. The exact solution satisfies the homogeneous jump conditions.

In Table 6.1 (a), we show a grid refinement analysis of our computations. The first column $E_N = \|u - u_h\|_\infty$ is the error of the finite-element solution measured in the L^∞ norm, and the second column is the estimate of the order of accuracy using the formula

$$\text{order} = \frac{\log(\|E_N\|_\infty / \|E_{2N}\|_\infty)}{\log 2}.$$

The sixth and eighth columns are defined as

$$e_{x,\infty} = \left\| \frac{\partial u}{\partial x} - \frac{\partial I_h u}{\partial x} \right\|_{\Omega', \infty}, \quad e_{y,\infty} = \left\| \frac{\partial u}{\partial y} - \frac{\partial I_h u}{\partial y} \right\|_{\Omega', \infty},$$

respectively. We see clearly the second order accuracy. The fourth to the last columns are the interpolation errors. We see that the interpolation errors are of second order and its derivatives are of first order. These are optimal.

In Table 6.1 (b), we show the results and comparison of the finite-element solution in L^∞ , L^2 , and H^1 norms. We see second order convergence in L^∞ and L^2 norms and first order in the H^1 norm as expected.

Example 2. A complicated interface and nonhomogeneous jump conditions. We consider the problem (1.1)–(1.5) with $\Omega = (-1, 1) \times (-1, 1)$ and the interface Γ being the zero level set of the function

$$\varphi(x, y) = \sqrt{x^2 + y^2} - 0.1 \sin(5\theta - \pi/5) - 0.5,$$

where $\tan \theta = x/y$ and $0 \leq \theta \leq 2\pi$; see Figure 6.1 for the geometry. The function β is defined by

$$\beta(x, y) = \begin{cases} x^2 + y^2 + 1 & \text{if } (x, y) \in \Omega^-, \\ b & \text{otherwise,} \end{cases}$$

where $b > 0$ is a parameter. The function f is defined by

$$f(x, y) = \begin{cases} -4(2x^2 + 2y^2 + 1) & \text{if } (x, y) \in \Omega^-, \\ 2 \sin x \cos y & \text{otherwise.} \end{cases}$$

TABLE 6.1

A grid refinement analysis for Example 1, where p_i are the approximated convergence order and the norms that involve the partial derivatives, $e_{x,\infty} = \|\frac{\partial u}{\partial x} - \frac{\partial I_h u}{\partial x}\|_{\Omega',\infty}$ and $e_{y,\infty} = \|\frac{\partial u}{\partial y} - \frac{\partial I_h u}{\partial y}\|_{\Omega',\infty}$. (a) The finite-element solution error and the interpolation error. (b) Results and comparison of the finite-element solution errors in $L^\infty(\Omega')$, $L^2(\Omega')$, and $H^1(\Omega')$ norms, where $\Omega' = \Omega \setminus \sum T_r$.

(a)

| N | $\ u - u_h\ _\infty$ | p_1 | $\ u - I_h u\ _\infty$ | p_2 | $e_{x,\infty}$ | p_3 | $e_{y,\infty}$ | p_4 |
|-----|-----------------------|-------|------------------------|-------|-----------------------|-------|-----------------------|-------|
| 32 | $1.314 \cdot 10^{-3}$ | | $2.590 \cdot 10^{-3}$ | | $1.056 \cdot 10^{-1}$ | | $1.043 \cdot 10^{-1}$ | |
| 64 | $4.215 \cdot 10^{-4}$ | 1.64 | $6.799 \cdot 10^{-4}$ | 1.93 | $5.351 \cdot 10^{-2}$ | 0.98 | $5.351 \cdot 10^{-2}$ | 0.96 |
| 128 | $1.008 \cdot 10^{-4}$ | 2.06 | $1.780 \cdot 10^{-4}$ | 1.93 | $2.754 \cdot 10^{-2}$ | 0.96 | $2.754 \cdot 10^{-2}$ | 0.96 |
| 256 | $2.729 \cdot 10^{-5}$ | 1.88 | $4.501 \cdot 10^{-5}$ | 1.99 | $1.391 \cdot 10^{-2}$ | 0.99 | $1.393 \cdot 10^{-2}$ | 0.99 |
| 512 | $7.697 \cdot 10^{-6}$ | 2.03 | $1.138 \cdot 10^{-5}$ | 1.99 | $6.999 \cdot 10^{-3}$ | 0.99 | $6.999 \cdot 10^{-3}$ | 0.99 |

(b)

| N | $\ u - u_h\ _\infty$ | p_5 | $\ u - u_h\ _{L^2}$ | p_6 | $\ u - u_h\ _{H^1}$ | p_7 |
|-----|------------------------|-------|------------------------|-------|------------------------|-------|
| 32 | 1.314×10^{-3} | | 6.500×10^{-4} | | 5.777×10^{-2} | |
| 64 | 4.215×10^{-4} | 1.64 | 1.597×10^{-4} | 2.03 | 2.661×10^{-2} | 1.12 |
| 128 | 1.008×10^{-4} | 2.06 | 4.001×10^{-5} | 2.00 | 1.345×10^{-2} | 0.99 |
| 256 | 2.729×10^{-5} | 1.88 | 9.899×10^{-6} | 2.01 | 6.593×10^{-3} | 1.03 |
| 512 | 6.697×10^{-6} | 2.03 | 2.489×10^{-6} | 1.99 | 3.289×10^{-3} | 1.00 |

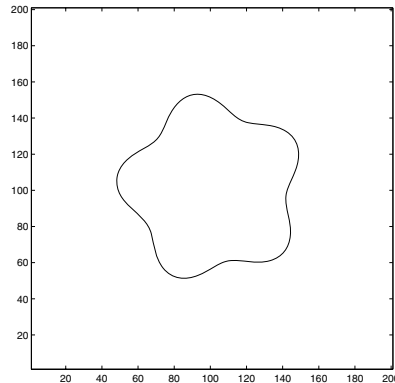


FIG. 6.1. The domain and the interface for Example 2.

Both β and f have nonzero jumps across the interface Γ . The exact solution is

$$u(x, y) = \begin{cases} x^2 + y^2 & \text{if } (x, y) \in \Omega^-, \\ \frac{1}{b} \left(\sin x \cos y + \log \sqrt{x^2 + y^2} \right) & \text{otherwise.} \end{cases}$$

Notice that both the solution u and the normal flux $\beta \partial_n u$ have nonzero jumps across the interface Γ .

We remark that the solution behavior depends on the magnitude of the parameter b . If b is large, then the solution is close to a piecewise quadratic function. If b is small, then the jumps of the solution and its normal flux across the interface are very large. Numerically, this gives rise to difficulties in achieving optimal convergence

properties [1, 16]. We test our method for various b and analyze the computed results.

In Table 6.2, we show a grid refinement analysis for $b = 100$. We see clearly the second order accuracy in L^∞ and L^2 norms and first order accuracy in the H^1 norm.

TABLE 6.2

A grid refinement analysis for Example 2 with $b = 100$, where p_i are the approximated convergence order and the norms that involve the partial derivatives. Second order accuracy in L^∞ norm is observed.

| N | $\ u - u_h\ _\infty / \ u\ _\infty$ | p_1 | $\ u - u_h\ _{L^2}$ | p_2 | $\ u - u_h\ _{H^1}$ | p_3 |
|-----|-------------------------------------|-------|-------------------------|-------|-------------------------|-------|
| 32 | 1.1995×10^{-1} | | 1.6705×10^{-2} | | 3.9175×10^{-1} | |
| 64 | 2.4397×10^{-2} | 2.30 | 1.8542×10^{-3} | 3.17 | 1.9551×10^{-1} | 1.00 |
| 128 | 5.3913×10^{-3} | 2.18 | 3.2668×10^{-4} | 2.51 | 9.8144×10^{-2} | 0.99 |
| 256 | 1.1218×10^{-3} | 2.27 | 5.1452×10^{-5} | 2.66 | 4.9894×10^{-2} | 0.94 |
| 512 | 2.7480×10^{-4} | 2.03 | 9.4668×10^{-6} | 2.44 | 2.5310×10^{-2} | 0.98 |

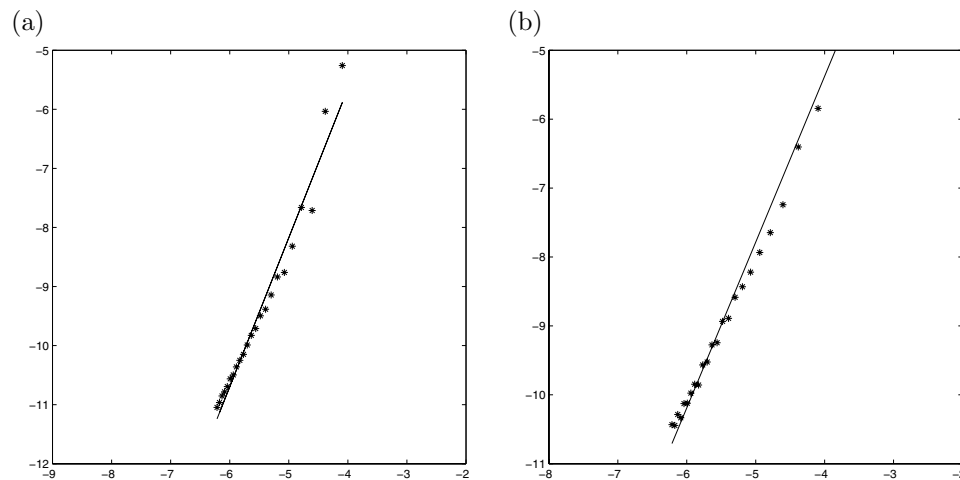


FIG. 6.2. The linear regression analysis in the L^∞ norm in log-log scale with the mesh varying according to $N = 40 + 20k$, $k = 0, 1, \dots, 23$. (a) $b = 1$; the slope (convergence order) is 2.8122. (b) $b = 0.1$; the slope is 2.4061.

Where b gets smaller, the jumps in the solution and flux get larger. For interface problems, the errors obtained from non-body-fitted meshes usually do not decrease monotonically as we refine the mesh; see, for example, [15]. For small b , it is thus more realistic to find the asymptotic convergence rate as the slope of the line fitting of the experimental data $(\log(h_i), \log(E_i))$.

In Figure 6.2, we show the linear regression analysis for $b = 1$ and $b = 0.1$ for the computed finite-element solution. For these two cases, the convergence orders are 2.8122 and 2.4061. As the mesh gets finer, the linear regression analyses (by deleting the results from coarse meshes) get closer to number two, indicating a second order accuracy. In Figure 6.3, we also show the linear regression analysis in the L^2 and H^1 norms. The convergence orders are 1.9906 and 0.9135, respectively.

Figure 6.4 shows the result for $b = 0.01$ that is quite small, and hence there is a large ratio in the coefficient from both sides of the interface. The convergence order from the sample meshes ranging from 40 to 500 with 10 increments is 1.8875; see Figure 6.4(a). But as the mesh gets finer, the linear regression analyses done by cutting the results from coarse meshes get closer to number two, again indicating a second order accuracy. Figure 6.4(b) shows the convergence order to be 1.9811.

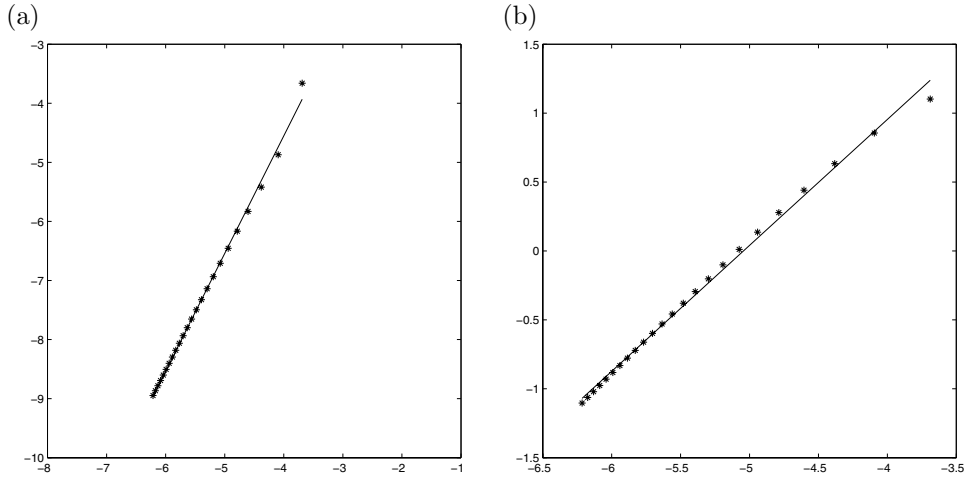


FIG. 6.3. The linear regression analysis in the L^2 norm (a), and in H^1 norm (b), in log-log scale with the mesh varying according to $N = 40 + 20k$, $k = 0, 1, \dots, 23$, $b = 1$. The slope (convergence order) is 1.9906 and 0.9135, respectively.

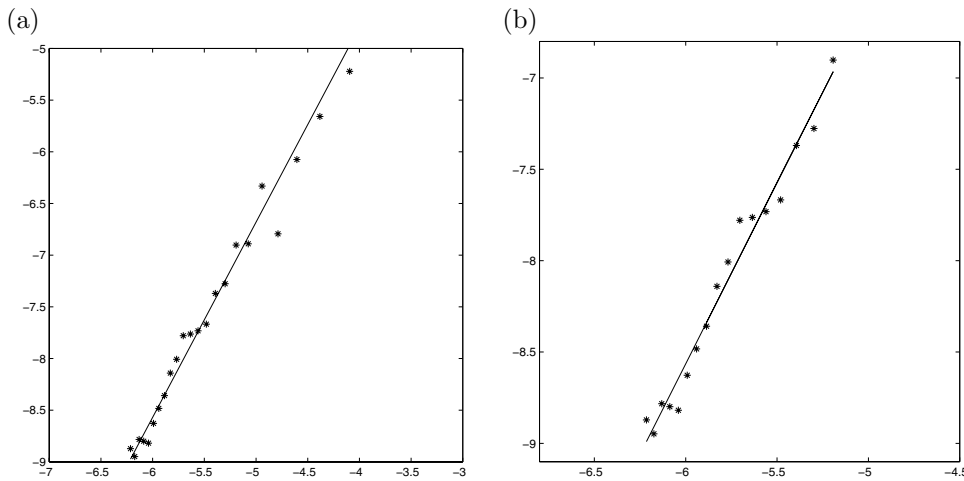


FIG. 6.4. The linear regression analysis in the L^∞ norm in log-log scale for $b = 0.01$. (a) $N = 40 + 20k$, $k = 0, 1, \dots, 23$; the slope (convergence order) is 1.8875. (b) $N = 40 + 20k$, $k = 1, 15, \dots, 23$; the slope is 1.9811.

7. Conclusions. We have developed a class of immersed-interface finite-element methods for solving elliptic interface problems with *nonhomogeneous jump conditions*. These methods consist of three parts:

- (a) a weak formulation of the problem in which the nonhomogeneous jump conditions are removed by using the level-set representation of the interface;
- (b) construction of immersed-interface finite-element basis functions for irregular nodes that satisfy the homogeneous jump conditions; and
- (c) several techniques of numerical implementation for the resulting finite-element equations.

Our methods have several advantages. For instance, they result in symmetric positive definite systems of linear equations. Moreover, they can be used with the level-set method for fast simulations of interface dynamics. Our basic error analysis and numerical tests demonstrate that such methods have optimal convergence properties.

REFERENCES

- [1] L. ADAMS AND Z. LI, *The immersed interface/multigrid methods for interface problems*, SIAM J. Sci. Comput., 24 (2002), pp. 463–479.
- [2] R. ADAMS, *Sobolev Spaces*, Academic Press, New York, 1975.
- [3] E. BÄNSCH, F. HAUSSER, O. LAKKIS, B. LI, AND A. VOIGT, *Finite element method for epitaxial growth with attachment-detachment kinetics*, J. Comput. Phys., 194 (2004), pp. 409–434.
- [4] S. C. BRENNER AND L. R. SCOTT, *The Mathematical Theory of Finite Element Methods*, 2nd ed., Springer-Verlag, New York, 2002.
- [5] W. K. BURTON, N. CABRERA, AND F. C. FRANK, *The growth of crystals and the equilibrium of their surfaces*, Phil. Trans. Roy. Soc. London Ser. A, 243 (1951), pp. 299–358.
- [6] R. E. CAFLISCH AND B. LI, *Analysis of island dynamics in epitaxial growth of thin films*, Multiscale Model. Simul., 1 (2003), pp. 150–171.
- [7] Z. CHEN AND J. ZOU, *Finite element methods and their convergence for elliptic and parabolic interface problems*, Numer. Math., 79 (1998), pp. 175–202.
- [8] P. G. CIARLET, *The Finite Element Method for Elliptic Problems*, North-Holland, Amsterdam, 1978.
- [9] A. DEMLOW AND G. DZIUK, *An adaptive finite element method for the Laplace–Beltrami operator on implicitly defined surfaces*, SIAM J. Numer. Anal., 45 (2007), pp. 421–442.
- [10] P. GREMAUD, C. KUSTER, AND Z. LI, *A study of numerical methods for the level set approach*, Appl. Numer. Math., 57 (2007), pp. 837–846.
- [11] P. GRISVARD, *Elliptic Problems in Nonsmooth Domains*, Pitman Advanced Publishing Program, Boston, MA, 1985.
- [12] S.-M. HOU AND X.-D. LIU, *A numerical method for solving variable coefficient elliptic equation with interfaces*, J. Comput. Phys., 202 (2005), pp. 411–445.
- [13] J. N. ISRAELACHVILI, *Intermolecular and Surface Forces with Applications to Colloidal and Biological Systems*, 2nd ed., Academic Press, New York, 1990.
- [14] C. JOHNSON, *Numerical Solution of Partial Differential Equations by the Finite Element Method*, Cambridge University Press, Cambridge, UK, 1987.
- [15] Z. LI, *A fast iterative algorithm for elliptic interface problems*, SIAM J. Numer. Anal., 35 (1998), pp. 230–254.
- [16] Z. LI AND K. ITO, *Maximum principle preserving schemes for interface problems with discontinuous coefficients*, SIAM J. Sci. Comput., 23 (2001), pp. 339–361.
- [17] Z. LI AND K. ITO, *The Immersed Interface Method: Numerical Solutions of PDEs Involving Interfaces and Irregular Domains*, Frontiers Appl. Math. 33, SIAM, Philadelphia, 2006.
- [18] Z. LI, T. LIN, AND X. WU, *New Cartesian grid methods for interface problem using finite element formulation*, Numer. Math., 96 (2003), pp. 61–98.
- [19] Z. LI, W.-C. WANG, I.-L. CHERN, AND M.-C. LAI, *New formulations for interface problems in polar coordinates*, SIAM J. Sci. Comput., 25 (2003), pp. 224–245.
- [20] S. OSHER AND R. FEDKIW, *Level Set Methods and Dynamic Implicit Surfaces*, Springer-Verlag, New York, 2002.

- [21] S. OSHER AND J. SETHIAN, *Front propagation with curvature dependent speed: Algorithms based on Hamilton-Jacobi formulations*, J. Comput. Phys., 79 (1988), pp. 12–49.
- [22] J. A. SETHIAN, *Level Set Methods and Fast Marching Methods*, 2nd ed., Cambridge University Press, Cambridge, UK, 1999.
- [23] D. YOUNG AND D. KINCAID, *The ITPACK package for large sparse linear systems*, in Elliptic Problem Solvers, M. Schultz et al., eds., Academic Press, New York, 1981, pp. 163–185.